Probing the buckling of axially compressed cylindrical shells: Stability landscape and nondestructive prediction

Kshitij K. Yadav[1], Zoe Sloane[2],Simos Gerasimidis[3]

Abstract
The buckling capacity of thin cylindrical shells depends on the underlying imperfections, which are generally unknown. As a result, cylindrical shells are designed conservatively using the knockdown factor approach that accommodates the uncertainties associated with underlying imperfections. Nevertheless, the quest for inexpensive high-fidelity estimates of the buckling capacity of thin cylindrical shells has been continued for a long time. Recent studies show that the methods based on the stability landscape of thin shells have the potential for capacity prediction without measuring the underline imperfections. The stability landscape is obtained by probing axially compressed cylindrical shells in the radially inward direction, and the location of the probing plays a crucial role in the accuracy of the prediction. In this study, the effect of the location of probing is investigated in the context of prediction accuracy. Further, a zone of influence of imperfections is defined such that if the probing is done in the zone of influence, the prediction will be accurate. Overall, this study reveals many aspects of the probing of axially compressed cylindrical shells: 1) probing can be used to predict the buckling capacity, 2) the probing location plays a crucial role in the accuracy of the prediction, and 3) a zone of influence of imperfections can be defined for accurate prediction of the buckling capacity of thin cylindrical shells.

1. Introduction
Thin shells are inherently optimal structures, and they, particularly cylinders and spheres, are widely used in many diverse applications ranging from aircraft fuselages to roofs of large buildings and from boat hulls to tall wind turbine towers. However, the optimization of thin shells comes with a cost— thin cylindrical shells are highly sensitive to imperfections (Koiter 1945). Imperfections, even relatively small, reduce the load-carrying capacities of thin shells significantly. The reduction in the load-carrying capacity depends on the size and the shape of underlying imperfections. Obtaining information about the underlying imperfection is difficult and expensive; as a result, the exact capacity of imperfect shells is unknown. Due to the lack of an inexpensive high-fidelity prediction method, thin shells are designed by the conservative knockdown factor method is an empirical method developed by NASA (NASA, 1965) in the late sixties after extensive experimental programs.

---

[1] Graduate Research Assistant, University of Massachusetts Amherst, <kkyadav@umass.edu>
[2] Graduate Research Assistant, University of Massachusetts Amherst, < zsloane@umass.edu >
[3] Assistant Professor, University of Massachusetts Amherst, <sgerasimidis@umass.edu >

Nevertheless, the full engineering potential of thin shells is still not being exploited. There are three potential approaches by which we can design thin shells efficiently: 1) making thin shells imperfection insensitive, 2) developing an inexpensive high-fidelity method that predicts the capacity of thin shells accurately without measuring the imperfections, and 3) coming up with a low-cost imperfection measurement device. Attempts have been made in all three directions; nonetheless, the development of the second approach, i.e., developing a high-fidelity prediction method, is recently getting intense attention. Indeed, a promising new framework based on the probing of axially compressed shells has emerged for the prediction of the buckling capacity of thin shells without complete knowledge of the shell's underlying imperfections (Thompson 2015, Thompson et al. 2016, Thompson et al. 2017, Hutchinson et al. 2017, Kreilos et al. 2017, Marthelot et al. 2017, Virot et al. 2017, Hutchinson et al. 2018, Fan 2019, Abramian et al. 2020, Yadav et al. 2021, Yadav et al. 2021, Nicholas et al. 2021). Yadav et al. (2021) has proposed a non-destructive technique for the evaluation of thin cylindrical shells' axial buckling capacity based on stability landscape. This procedure consists of three steps: 1) shells are put under axial compression Fa, 2) these axially compressed shells are probed in the radial direction at the location of a pre-existing imperfection, and 3) the peak probe force F_p^{max} and the corresponding axial compression F_a are recorded and used to predict the buckling axial capacity. For a detailed explanation of the procedure, refer to Yadav et al. (2021). The study of Yadav et al. (2021) has established that if the probing is done at the right location, i.e., at the dominant imperfection, the capacity can be predicted accurately. However, two issues are remains to be resolved: 1) how to define the right location and 2) how to identify the right location. Ankalhope and Jose (2021) has proposed that the right location for the probing is the least resistant path, and that location can be found by probing at multiple locations.

In this study, we computationally (FEM) investigated the importance of the location of probing in the context of the accuracy of prediction. First, the probing profiles, i.e., the plot of the peak probe force F_p^{max} and the corresponding axial compression F_a, are created for imperfect cylinders by probing away from the imperfection. Next, these probing profiles are compared with the probing profile of perfect, and the profile of imperfect cylinder when probing is done at the imperfection. Next, based on the profile comparison, a zone of influence i.e., the area around the imperfection that gives accurate prediction if probing is done within the area, is identified. Finally, the paper is concluded by noticing the main findings of this study.

2. Finite element modeling and description of imperfection

For this study, a cylinder with dimple-like geometric imperfection is analyzed computationally using FEA package ABAQUS [1]. The cylinder represents mini Coke cans (7.5 fl oz), made of aluminum, and chosen in the anticipation of future experiments. The dimensions and material properties of the cylinder are given in Table 1. Further, we simplified our modeling assuming the cross-sections of cans are circular throughout the length, which is a slight deviation from the real cans. For meshing, around 20000 four node reduced integration shell (*S4R*) elements are created, utilizing four integration points along the thickness of each element. Fig. 1 demonstrates the Finite Element Modeling and boundary conditions. For compressing the cylinder to a prescribed axial compression, two nodes are defined at the center of the top and bottom cross-sections of the cylinder; we call them center nodes. Rigid links are created to connect the nodes at the end of the cylinder to the respective center nodes to constrain the displacements U_1, U_2, and U_3, and rotations

2

UR$_1$, UR$_2$, and UR$_3$ of the nodes at the end from moving and rotating with respect to the center nodes. Using these constraints one end of the cylinder is clamped by fixing the central node at z = 0. At the other end (z = L) a clamped boundary condition is enforced, but the end of the cylinder is loaded by applying an axial displacement U$_3$ = -Δ till the axial compression reached the prescribed value as shown in Fig. 1. Once the cylinder is loaded under the prescribed axial compression, the probing force, directed toward the center of the cross-section, is applied as shown in Fig.2.

Table 1: Dimensions and the material properties of the can

R	L	R/t	E	ν
(mm)	(mm)		(Gpa)	
28.6	107	286	68.95	0.3

The dimple imperfection is modeled as a two-dimensional normal distribution function following Gerasimidis et al. (2018) and Yadav and Gerasimidis (2019). The mathematical description of the dimple imperfection is given as follows:

$$w = -\delta e^{\left(\frac{x-x_0}{L_1}\right)^2} e^{\left(\frac{\theta-\theta_0}{\theta_1}\right)^2} \tag{1}$$

where w represents the deviation from the original position in the radial direction, δ is the amplitude of the imperfection, x and θ are the axial and circumferential coordinates (x0 and θ0, respectively) are the center of the dimple whose values are chosen such that the dimple is located in the middle section of the cylinder. L_1 and θ_1 are the parameters that dictate the length (in the axial direction) and the width (in the circumferential direction) of the dimple. In this study, the value of L1 and θ1 are 0.55λ and 0.55λ/R (Gerasimidis et al. 2018), where λ is the half-wavelength of classical axisymmetric buckling mode of the cylindrical shell under axial load, and its value is given by Eq. (2) (Timoshenko et al. 1961).

$$\lambda = \pi \sqrt{\frac{Rt}{\sqrt{12(1-v^2)}}} \tag{2}$$
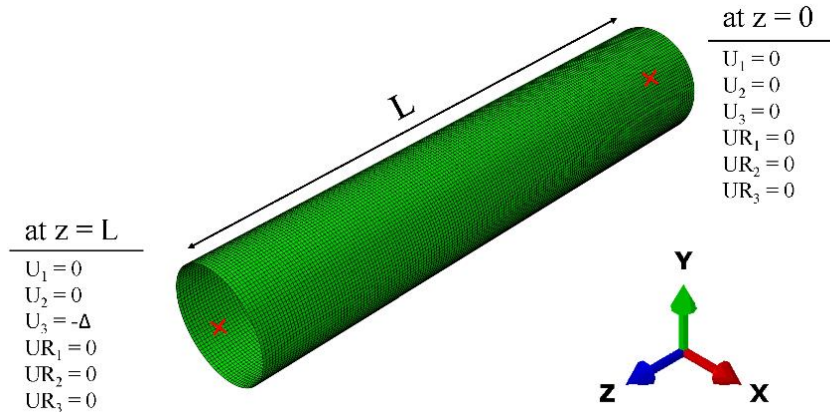

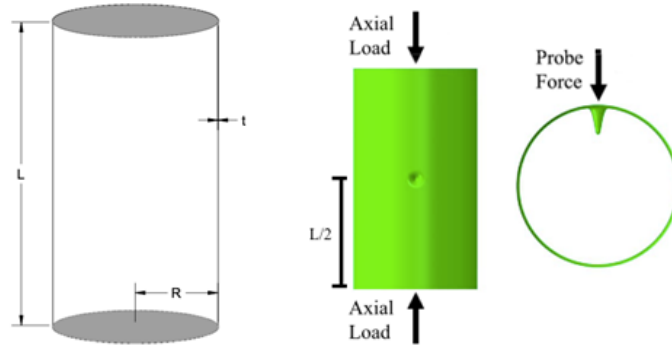Figure 1: Finite Element Model of the cylinder along with boundary conditions.

3

Figure 2: Probing of dimple-like the imperfect cylinder.

3. Result and Discussion

It was established that the prediction is accurate when the probing is done in the middle of the imperfection. However, for a real thin shell, the location of imperfections is unknown. Thus, evaluating the accuracy of predictions when probing away from the imperfections is essential. Moreover, finding a zone of influence i.e., if probing is done in the zone, the prediction will be accurate. around the imperfection, is key for developing a framework for non-destructive prediction of thin shells' capacity.
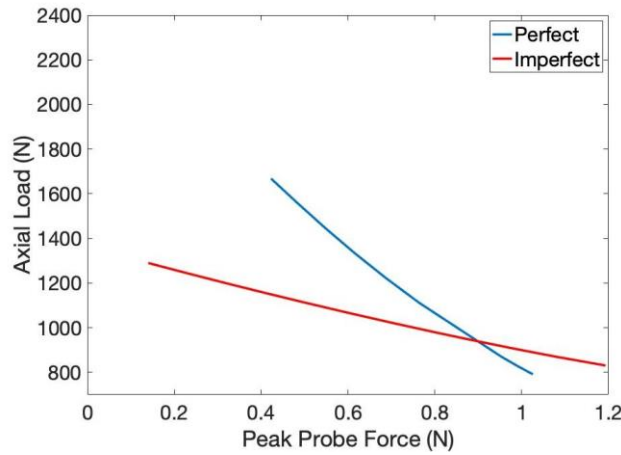

Figure 3: Plot between the peak probe force *Fpmax* and the corresponding axial compression *Fa* for the perfect cylinder and the imperfect cylinder when probing is done in the middle of the imperfection.

The primary objective of this study is to find the zone of influence of an imperfection. The zone of influence of an imperfection is defined as the area sounding the imperfection such that if probing is done in that area, the presence of the imperfection is detected, and prediction of capacity is accurate. In this study, we use a dimple with amplitude t as an imperfection, and the zone of influence of the imperfection is identified by comparing the probing profiles, i.e., the peak probe force F_p^{max} and the corresponding axial compression F_a. For the comparison of probing profiles, first the probing profiles of the perfect cylinder, and the probing profile of imperfect cylinder when probe at the middle of imperfection is found. Fig. 3 shows the plot between the peak probe force F_p^{max} and the corresponding axial compression F_a for the perfect cylinder and the imperfect

4

cylinder when probing is done in the middle of imperfection. The actual capacity of the perfect cylinder is 2622 *N* and of the imperfect cylinder is 1362. If the curves will be extended, they intersect *Y* axis near 2622 *N* for the perfect cylinder and near 1362 *N* for the imperfect cylinder. This means the probing gives an accurate prediction. Now, we probe away for the imperfection to find when the probing profile is following the probing profile of the perfect cylinder and when the profile is following the profile of the imperfect cylinder. These comparisons give the clue of the zone of influence.

3.1 Probing away from the imperfection along circumferential direction
To understand how the probing profile of the dimple-like imperfect cylinder is affected if not probed at the middle of the dimple, we create plots between the peak probe force *Fpmax* and the corresponding axial compression *Fa* for 16 probing locations along the circumferential direction. The angular distance of 16 locations form the middle of the dimple are: 1.840, 3.680, 5.520, 7.360, 9.200, 11.040, 12.880, 14.720, 16.560, 18.400, 20.240, 22.080, 23.920, 25.760, 27.600, and 29.440. Fig. 4a shows the probing profiles for these 16 locations along with the profile of the perfect cylinder and imperfect cylinder when the probe is done in the middle of the dimple. It can be seen that two regimes exist in Fig. 4a.
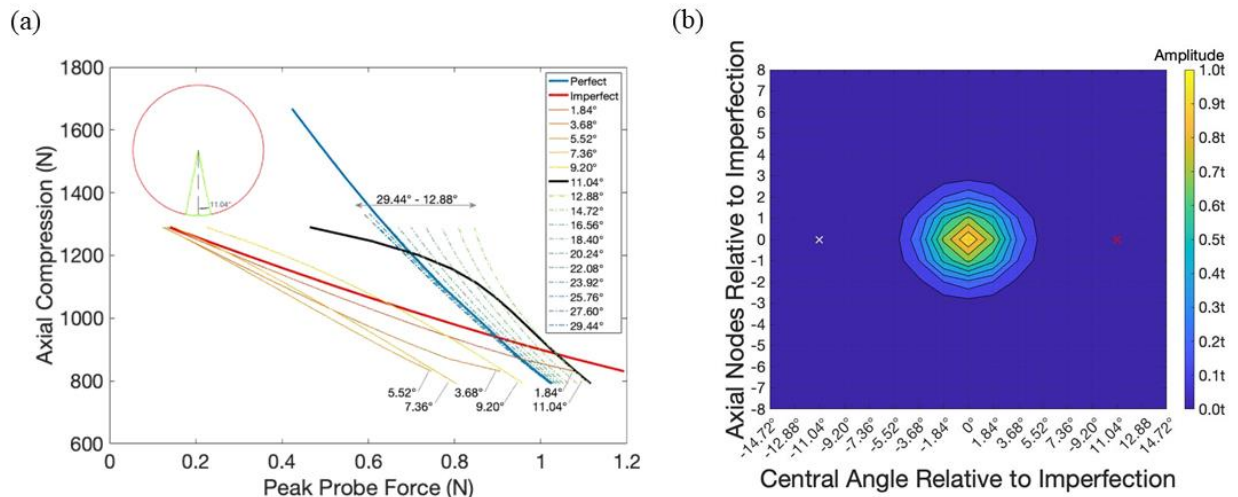

Figure 4: a) Probing profiles for these 16 locations along with the profile of the perfect cylinder and imperfect cylinder when the probe is done in the middle of the dimple. b) The limit of the zone of influence along the circumferential direction.

The first regime is the one when the location of probing is within 11.04^0 from the middle of the dimple, and the probing profiles follow the profile pattern of the imperfect cylinder. For the first regime, if the curves are extended, they intercept Y axis near 1362 *N,* which is the capacity of the imperfect cylinder. Thus, probing is able to detect the presence of imperfection and could be used to predict the capacity accurately even when probing is done 11.04^0 away from the middle of the dimple. The second regime is the one when the location of probing is outside 11.04^0 from the middle of the dimple, and the probing profiles follow the profile pattern of the perfect cylinder. For the second regime, if the curves are extended they intercept the Y axis near 2622 *N* or more than 2622 *N*. As a result, probing is unable to detect the presence of imperfection and if used for

the prediction, the prediction is inaccurate. At angle 11.04^0, transition takes place from one regime to another as shown in Fig. 4a. For small axial compression, the profile for 11.04^0 follows the profile pattern of the perfect cylinder, while for higher imperfection amplitude it is bending toward the profile pattern of the imperfect cylinder. 11.04^0 can be assumed as the limit of the zone of influence for the circumferential direction. Fig. 4b shows the contour of the imperfection around the dimple along with the extreme of the zone of influence along the circumferential direction.
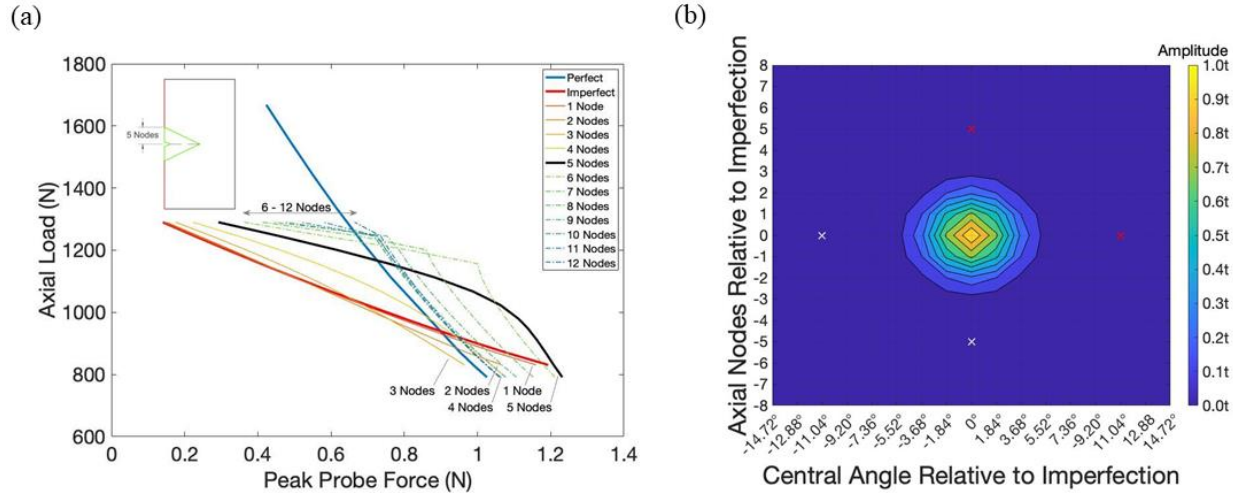

Figure 5: a) Probing profiles for these 12 locations along with the profile of the perfect cylinder and imperfect cylinder when the probe is done in the middle of the dimple. b) The limit of the zone of influence along the circumferential direction.

3.2 Probing away from the imperfection along axial direction

To find how the location of probing along the axial direction affects the probing profile, we probe away from the imperfection along the axial direction at 12 locations: Node1, Node2, Node3, Node4, Node5, Node6, Node7, Node8, Node9, Node10, Node11, and Node12. These locations are away from the middle of the dimple in multiple of 0.9386 *mm* i.e., Node1 is 1X 0.9386 *mm*, and Node 12 is 12X 0.9386 *mm* away from the middle of the dimple. Fig. 5 shows the probing profiles for these 12 locations along with the profile of the perfect cylinder and imperfect cylinder. Here again, two regimes exist.

The first regime is the one when the location of probing is less than 5x 0.9386 *mm* (Node5), and the probing profiles follow the profile pattern of the imperfect cylinder. For the first regime, if the curves are extended they intercept the Y axis near 1362 *N,* the capacity of the imperfect cylinder. Thus, probing is able to detect the presence of imperfection and could be used to predict the capacity accurately even when probing is done at 5x 0.9386 *mm* away from the middle of the dimple. The second regime is the one when the location of probing is outside 5x 0.9386 *mm*, and the probing profiles follow the profile pattern of the perfect cylinder. For the second regime, if the curves are extended, they intercept the Y axis near 2622 *N* or more than 2622 *N.* As a result, probing is unable to detect the presence of imperfection and if used for the prediction, the prediction is inaccurate. At distance 5x 0.9386 *mm*, transition takes place from one regime to another as shown in Fig. 5. For small axial compression, the profile for 5x 0.9386 *mm* (Node 5) follows the profile pattern of the perfect cylinder, while for higher imperfection amplitude it is

bending toward the profile pattern of the imperfect cylinder. 5x 0.9386 *mm* can be assumed as the limit of the zone of influence for the axial direction. Fig. 5b shows the contour of the imperfection around the dimple along with the extreme of the zone of influence along the circumferential direction and axial direction.

3.3 Probing away from the imperfection along circumferential-axial direction and zone of influence

We have established the axial and circumferential limits of the zone of influence in the previous subsections. Following the same procedure, we also found the limits of the zone of influence along the circumferential-axial direction that is when the probing is away from the imperfection along the diagonal direction. Fig. 6 shows the limit of the zone of influence of the dimple-like imperfection. The red crosses are the limit that is actually found. The white crosses are the extrapolation of the actual limits. Since the cylinder is symmetrical around the dimple, we only need to find the limits in one quarter. It can be seen that the zone of influence is a large area compared to the dimensions of the imperfections. This means that for a cylinder with unknown imperfections, we might need to probe more than one location (since we do not know the location of imperfection). However, fewer locations are needed as an imperfection has a large zone of influence.
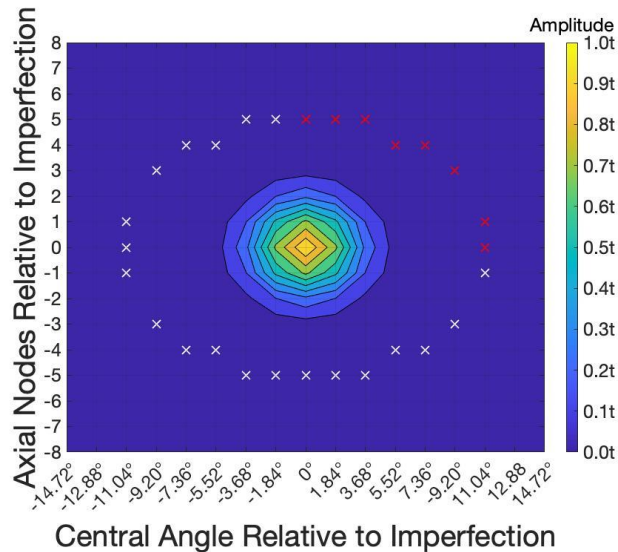

Figure 6: Zone of influence of the dimple with amplitude t.

4. Conclusions

We found that the zone of influence is a key feature of an imperfection in a thin cylindrical shell. If probing is done within the zone of influence, the prediction of the capacity of the shell will be accurate. Thus, the capacity prediction of a cylinder with unknown imperfections requires probing at multiple locations. Another notable feature of the zone of influence is that its size is significantly larger than the size of the imperfection. As a result, the capacity of a cylinder with unknown imperfections can be predicating by probing at very few locations. These results are very encouraging and suggest that a robust framework can be developed for predicting the capacity of the imperfect cylinder without the knowledge of the underline imperfections.

References

ABAQUS manual 6.14-14. Dassault Systèmes Simulia Corp.

Abramian A., Virot E., Lozano E., Rubinstein S. M., Schneider T. M., 2020., "Nondestructive prediction of the buckling load of imperfect shells." *Physical Review Letters*, 125 225504.

Ankalhope S, Jose S. "Non-destructive prediction of buckling load of axially compressed cylindrical shells using Least Resistance Path to Probing" *Thin-Walled Structures, 2022.*

Cuccia N., Yadav K.K., Virot E., Gerasimidis S., Rubinstein S.M. (2021), "Universal Features of Buckling Initiation in Thin Shells." *Bulletin of the American Physical Society*, 2021.

Fan H. (2019), "Critical buckling load prediction of axially compressed cylindrical shell based on non-destructive probing method." *Thin-Walled Structures*, 139 91-104.

Gerasimidis S., Virot E., Lee A., Hutchinson J.W., Rubinstein S.M. (2018), "On Establishing Buckling Knockdowns for Imperfection-Sensitive Shell Structures." *Journal of Applied Mechanics*, 85 (9) 091010.

Hutchinson J.W., Thompson, J.M.T. (2017), "Nonlinear Buckling Interaction for Spherical Shells Subject to Pressure and Probing Forces." *Journal of Applied Mechanics*, 84 (6) 061001.

Hutchinson J.W., Thompson, J.M.T. (2018), "Imperfections and energy barriers in shell buckling." *International Journal of Solids and Structures*, 148-149 167-168.

Koiter, W. T. (1945). "On the stability of elastic equilibrium." *Thesis Deft, H.J. Paris, Amsterdam.*

Marthelot J., Jiménez F.L., Lee A., Hutchinson J.W., Reis P.M. (2017), "Buckling of a Pressurized Hemispherical Shell Subjected to a Probing Force." *Journal of Applied Mechanics*, 84 (12) 121005.

NASA SP-8007 (1965). "Buckling of thin-walled circular cylinders."

Riks E. (1979), "An incremental approach to the solution of snapping and buckling problems." *International Journal of Solids and Structures*, 15(7) 529-551.

Thompson, J.M.T. (2015), "Advances in Shell Buckling: Theory and Experiments." *International Journal of Bifurcation and Chaos*, 25 (01) 153001.

Thompson, J.M.T., Sieber J. (2016), "Shock-Sensitivity in Shell-Like Structures: With Simulations of Spherical Shell Buckling." *International Journal of Bifurcation and Chaos*, 26 (02) 1630003.

Thompson, J.M.T., Hutchinson J.W., Sieber J. (2017), "Probing Shells Against Buckling: A Nondestructive Technique for Laboratory Testing." *International Journal of Bifurcation and Chaos*, 27 (14) 1730048.

Timoshenko S. P., Gere J.M. (1961) Theory of elastic stability. McGraw-Hill.

Virot E., Kreilos T., Schneider T.M., Rubinstein S.M. (2021), "Stability Landscape of Shell Buckling." *Physical Review Letters*, 119 224101.

Yadav K.K., Cuccia N., Virot E., Gerasimidis S., Rubinstein S.M. (2021), "A non-destructive technique for the evaluation of thin cylindrical shells' axial buckling capacity." *Journal of Applied Mechanics*, 2021.

Yadav K.K., Cuccia N., Virot E., Gerasimidis S., Rubinstein S.M. (2021), "Prediction of the buckling capacity of thin shells by using stability landscapes." *Bulletin of the American Physical Society*, 2021.

Yadav K.K., Gerasimidis S. "Instability of thin steel cylindrical shells under bending" *Thin-Walled Structures, 2019.*